IEEE Access
Multidisciplinary | Rapid Review | Open Access Journal

Received April 30, 2019, accepted May 28, 2019, date of publication May 30, 2019, date of current version June 10, 2019.

Digital Object Identifier 10.1109/ACCESS.2019.2920065

Joint Optimization of Area Throughput and Grid-Connected Microgeneration in UAV-Based Mobile Networks

LUCA CHIARAVIGLIO[1,2], (Senior Member, IEEE), FABIO D'ANDREAGIOVANNI[3,4], KIM-KWANG RAYMOND CHOO[5], (Senior Member, IEEE), FRANCESCA CUOMO[6], (Senior Member, IEEE), AND STEFANIA COLONNESE[6]

[1]Department of Electronic Engineering, University of Rome Tor Vergata, 00133 Rome, Italy
[2]Consorzio Nazionale Interuniversitario per le Telecomunicazioni, 00133 Rome, Italy
[3]National Center for Scientific Research (CNRS), 75016 Paris, France
[4]Sorbonne Universités, Université de Technologie de Compiègne, CNRS, 60200 Compiègne, France
[5]The University of Texas at San Antonio, San Antonio, TX 78249, USA
[6]DIET Department, University of Rome Sapienza, 00185 Rome, Italy

Corresponding author: Luca Chiaraviglio (luca.chiaraviglio@uniroma2.it)

This work was supported by the University of Rome Tor Vergata BRIGHT Project (Mission Sustainability Call).

ABSTRACT Small cells (SCs) mounted on top of the unmanned aerial vehicles (UAVs) are a promising solution to boost the capacity in hotspot areas. However, the adoption of UAV-SCs involves the planning of their missions over time, which includes the scheduling of recharging actions of each UAV-SC at ground sites. Typically, the energy needed to recharge UAV-SCs is derived from the grid, which can be coupled with microgeneration exploiting renewable energy sources (e.g., solar panels). In this architecture, the energy that is locally produced can be either sold to the grid or used to recharge the UAV-SCs. On the other hand, when the energy from microgeneration is insufficient for recharging the UAV-SCs, additional energy can be bought from the grid. In this paper, we investigate the trade-off between maximizing the throughput provided by the UAV-SCs over a set of areas, maximizing energy sold to the grid, and maximizing energy bought from the grid. The proposed model, MaxUAVProfit, is designed to (i) plan the UAV-SCs missions as a sequence of positions and actions in 3D space vs. time, (ii) manage the grid-connected microgeneration, and (iii) control the amount of throughput received by each hotspot. We then evaluate the MaxUAVProfit in a realistic scenario, which is based on the measurement of real cellular metrics and a realistic UAV-SC energy consumption model. Our findings demonstrate the superiority of the MaxUAVProfit with respect to other competing solutions, which include either optimization of microgeneration or maximization of the area throughput.

INDEX TERMS UAV-based networks, energy-management, mixed integer linear programming, renewable energy sources, cellular networks, energy and performance trade-offs.

I. INTRODUCTION

Unmanned aerial vehicles (UAVs) can potentially be used to provide small cell (SC) wireless connectivity in hotspot areas [1], [2]. In comparison to conventional fixed cellular networks, UAV-SCs introduce the following advantages: (i) improved throughput to areas covered by UAV-SCs, due to good channel conditions, coupled with dedicated UAV-SC radio resources, (ii) no fixed installation costs for UAV-SCs, and (iii) spatial and temporal flexibility, as UAV-SCs can easily move across physical territory to cover hotspot areas, as needed or on an ad-hoc basis. However, deploying UAV-SCs introduces an additional level of complexity, particularly due to the planning of UAV-SC missions [3]. This step, in fact, requires the scheduling of UAV-SCs actions and the computation of UAV-SCs trajectories over time and space [4]. In this context, a UAV-SC can perform a variety of actions, such as: moving (flying) over a territory, providing coverage of an area, and recharging on a ground site. The path of UAV-SCs in the 3D space needs to be carefully planned, for

The associate editor coordinating the review of this manuscript and approving it for publication was Hao Luo.

example in order to reach an area to be covered from a ground site.

Generally, UAV-SCs have limited battery capacity [5]. When the battery is depleted, the UAV-SC has to be recharged. The recharge is typically performed on a ground site, which hosts energy plugs at which the UAV-SC can be attached. The required energy can be derived from a variety of sources, such as a direct connection to the electricity grid and/or via some renewable energy sources. Grid-connected MicroGeneration (GMG) [6] is one popular option, where energy is locally generated from renewable energy sources (e.g., solar panels and/or wind turbines). However, in the event that locally produced energy is insufficient to meet the demand, additional energy can be bought from the grid. Similarly, additional unused locally produced energy can be sold to the grid. In other words, the owner of a GMG site can be producer and consumer of energy at the same time.

Managing a GMG site while taking into consideration the uncertain nature of UAV-mission is a challenging and complex task logistically. From a user quality of service (QoS) perspective, UAV-SCs should be used as much as possible, in order to maximize the coverage of hotspot areas, and consequently the throughput provided to a set of users. Such a strategy requires frequent recharging of UAV-SCs, thus limiting the amount of energy that can be sold to the grid, and perhaps incurring additional expenses to buy energy from the grid. From the GMG perspective, minimizing UAV-SC deployment can maximize energy sale to the grid, as well as minimize the purchase of additional energy from the grid.

The goal of this paper is to investigate this trade-off, an understudied research area in the literature. In particular, we attempt to answer the following research question: "How do we strike a balance between maximizing the throughput provided by UAV-SCs in a set of areas and the GMG energy consumption at ground sites?". Specifically, we propose a new optimization model, hereafter referred to as MaxUAVProfit. The proposed model is designed to: (i) plan the UAV-SCs missions in 3D space over a set of *time slots* (TSs), (ii) associate an action (e.g., moving, recharge, and covering) to each UAV-SC in each TS, (iii) strike an optimal balance between GMG and UAV-SCs in each TS, in terms of energy bought/sold from/to the grid, energy locally produced from microgeneration, and energy used to recharge the UAV-SCs, and (iv) evaluate the throughput provided to the areas with and without UAV-SCs. In the latter case (i.e., without UAV-SCs), basic coverage capabilities are provided by a fixed *macro cell* (MC).

The rest of the paper is organized as follows. Section II briefly reviews related literature. Sections III and IV present the UAV-SC architecture and the problem formulation, respectively. Section V describes the evaluation scenario. Section VI details our findings, showing that MaxUAVProfit outperforms prior solutions (that target either the maximization of UAV-SC coverage or the optimization of GMG energy). Section VII discusses the considered problem and the implementation issues. Finally, Section VIII concludes our work and presents future research directions.

II. RELATED WORK

In recent times, there have been attempts to integrate UAVs in (mobile) wireless networks. For example, in [7], UAVs with computing capabilities are integrated in a mobile cloud computing system. In this way, mobile users can exploit UAVs to offload their computation. In [8], UAVs are used for wireless power transfer. To this end, the UAVs are equipped with energy transmitters and they can move across an area to recharge a set of receivers (e.g., part of an Internet of Things (IoT) wireless networks).

Concerning the use of UAVs as flying base stations (BSs), we refer the interested reader to [1], [2], [9] for discussions on associated benefits, challenges and opportunities. For example, UAV-SCs can be used to improve coverage and network connectivity in different contexts, such as rural areas [3] and emergency situations [10].

There are a number of challenges associated with UAV-SCs, such as optimal path planning (i.e., determining optimal flight paths for UAVs). In the context of this paper, UAV flight path and movements can have an impact on the quality of the provided wireless connection. Specifically, a number of studies have analyzed the optimal placement of UAVs in a 3D environment [11]–[13], although only a very small number of studies have focused on UAV trajectory planning by taking into consideration both UAVs dynamics and the communication service offered through a small cell mounted on the UAV [14], [15]. For example, the authors in [11] presented a 3D placement solution for UAV-SCs that included additional decision variables to relate the altitude of the UAV-SC to the radius of the coverage area, whereas the authors in [12] defined an optimization model for 3D placement that maximizes the number of covered users, while taking into account the minimal transmission power required. In [13], it is shown that the UAV-SC placement can impact the QoS when this solution is used to provide limited-delay video streaming to mobile users.

Focusing on the path planning aspects, the authors in [14] proposed an energy-aware path planning algorithm, which considers factors such as camera sampling period and spatial resolution for pictures. In a separate work, the authors in [15] proposed a flow-based optimization model to integrate path planning and recharging of UAVs with a city bus fleet. In yet another work, the authors in [5] proposed an optimization model and a solution algorithm for UAV positioning and recharging scheduling for covering an area. However, none of these studies considers the impact of UAVs on GMG.

There have also been studies focusing on leveraging renewable energy sources in cellular networks [16]–[18]. In [17], for example, the potential of using a cellular network based on a solar panel system is analyzed. Moreover, as pointed out by [18], a more realistic solution is to integrate renewable energy sources with the grid (e.g., via a direct connection). This aspect is also exploited by our work, in order to:

i) mitigate the risk due to the intermittent nature of renewable energy sources, ii) manage energy demand changes, and iii) (possibly) maximize the financial payoff (e.g., by selling excess energy to the grid). However, we point out that [16]–[18] assume a cellular network composed of fixed BSs, and not UAV-SCs like in our work, thus resulting in a completely different problem.

Seeking to address the limitations in existing literature, in this paper we focus on the following innovative aspects:

- we consider a GMG system to provide the required amount of energy to recharge UAV-SCs;
- we model the UAV-SC missions over the 3D space, by considering a detailed UAV-SC mission model that integrates a wide range of UAV-SC actions (e.g., recharging, moving, and covering) and positions in the space;
- we precisely model the UAV-SC energy consumption, which is impacted by parameters such as distance between current and intended positions, UAV-SC weight, size of UAV-SC rotors, altitude and current UAV-SC action;
- we consider a scenario where the basic cellular coverage provided by the MC is measured from a real cellular network deployed over the territory;
- we present a model for Radio Resource Management (RRM) at the MC, by considering the radio resources released when an area is served by a UAV-SC (these resources can be used to improve the throughput to areas not covered by the UAV-SC);
- we jointly manage both GMG energy and throughput from UAV-SCs to a set of areas, and we study the impact of weighing differently these two terms.

III. ARCHITECTURE

In our architecture, we consider a set of UAV-SCs and one MC providing mobile service over a part of the territory. A set of areas is then selected in the MC service area, for example by considering hotspot zones. In addition, MC equipment is hosted at a ground site, which is also used as a UAV-SC parking station (i.e., it provides GMG energy capabilities to UAV-SCs).

A. CASE STUDIES

Two representative case studies are presented in Fig. 1, where we consider four hotspots in the MC service area. In Fig. 1(a), no UAV-SC is used (e.g., parked at ground site in stand-by mode). Thus, mobile service is solely provided by MC. The RRM feature implemented by MC assigns radio resources, by handling the requests from users and/or specific rules defined by the operator (e.g., in order to provide large amount of resources to specific users). However, we expect that significant radio resources are assigned to the hotspot areas, which are the zones where user activity and/or density tend to concentrate. In Fig. 1(b), two UAV-SCs are used to cover Hotspots 1 and 2. In this case, dedicated radio resources are provided by UAV-SCs to serve the users in hotspot areas,

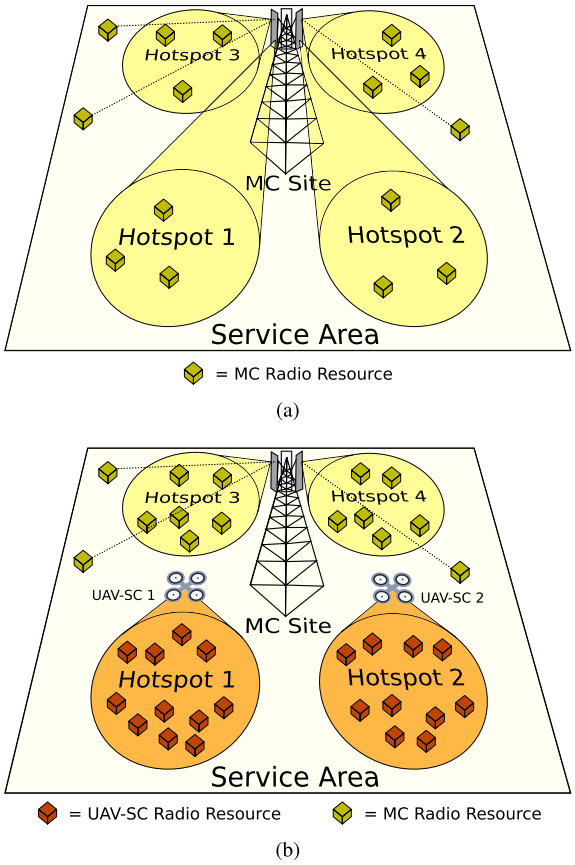

FIGURE 1. Management of radio resources of Macro Cell (MC) and unmanned aerial vehicles-based small cells (UAV-SCs). In case (a), no UAV-SC is used and the service is only provided by MC. The radio resource management (RRM) of MC assigns the radio resources over a service area, including four hotspots. In case (b), two UAV-SCs cover Hotspots 1 and 2. MC radio resources previously used to serve Hotspots 1 and 2 in case (a) are reallocated to improve the capacity of Hotspots 3 and 4 in case (b).

with the aim of providing improved QoS. Moreover, the introduction of UAV-SCs is beneficial to the MC. In particular, different radio resources of the MC (previously assigned to Hotspots 1 and 2) are reallocated to the set of users in Hotspots 3 and 4. This also positively impacts their QoS.

B. BASIC ASSUMPTIONS

In our work, we take into account the improvement in terms of capacity brought by UAV-SCs, and the redistribution of MC radio resources, by deploying UAV-SCs. Specifically, we consider bandwidth as the main resource managed by RRM. Moreover, we consider the bandwidth variation globally assigned to an area, and not to single users. Actually, evaluating the distribution of radio resources to single users inevitably complicates the problem, making it very challenging to be solved even for small problem instances.[1] Therefore, we consider the bandwidth distribution over a set of areas.

[1]We refer the interested reader to the work of Wu *et al.* [19], which faces the joint trajectory and communication design of UAV-based networks. We also point out that the problem in [19] does not consider the GMG aspects, which are instead taken into account by our work.

The actual bandwidth distribution to single users may be done as a second step (by considering e.g., the specific service requested by each user). We leave the investigation of this last aspect as future work.

Another aspect assumed in this work is that the bandwidth provided by the UAV-SC is separated from the one provided by the MC. In fixed BS deployments, in fact, SCs are used to boost the capacity in dense regions, where the users tend to concentrate. To achieve this goal, SCs employ higher frequencies compared to the ones used by MCs [20], [21]. In this way, the spectrum of the SC is separated from the one of the MC. This assumption is corroborated by existing deployments of SCs offered by telecom manufacturers [22], [23] and by current frequency assignments of LTE networks (see e.g., [24] for the Italian case). In our work, therefore, the UAV-SC bandwidth is separated from the MC one. In this way, the impact of interference between the MC and the UAV-SC can be neglected.

Eventually, we assume that the set of areas, which is an input to our problem, is designed in such a way to limit the interference between neighboring areas served by different UAV-SCs. Moreover, we assume that the radio link that needs to be established between the UAV-SC and the ground site providing connectivity with the rest of the network is reliable. To this aim, we enforce a maximum distance constraint between a UAV-SC covering an area and a ground site at which the UAV-SC is connected.

Finally, we assume that each UAV-SC covers an area with a circle shape and a radius in the order of hundreds of meters. On the other hand, we assume that the coverage area of the MC is in the order of square kilometers. Clearly, the area covered by the UAV-SC depends on the features of the antenna mounted on board, such as the coverage pattern, the directionality and the tilting. In this work, we have assumed the exploitation of omni-directional antennas to realize the SC, which is a common assumption in the literature (see e.g., [25], [26]). Clearly, the size of the coverage area of the UAV-SC has an impact on the throughput achievable by each user, due to the fact that the radio resources over an area are then split among the users. A large area, in fact, may include a huge number of users, leading to a relatively low throughput to each user even if a UAV-SC is exploited. On the other hand, a small area may be composed of few users, each of them receiving a large throughput when served by the UAV-SC. However, we point out that targeting the evaluation of the throughput for each user introduces an additional level of complexity, which we plan to address as future work.

C. AREA THROUGHPUT COMPUTATION

Each UAV-SC provides dedicated radio resources to an area. Therefore, no radio resources from the MC are delivered to an area when the area is served by the UAV-SC. In this context, the radio resources that were previously assigned to the area (when was exclusively served by the MC) can be released to the MC, and redistributed to the areas that are not covered by any UAV-SC. In this way, each area served solely by the MC receives an amount of baseline bandwidth, plus an additional bandwidth that has been released by the areas that are currently served by UAV-SCs. More formally, the throughput $R_{(a,t)}$ of area a served by MC at Time Slot (TS) t is expressed as:

$$R_{(a,t)} = \alpha \cdot \eta(c^{\mathrm{MC}}_{(a,t)}) \cdot [\lambda^{\mathrm{BASE}}_{(a,t)} + \lambda^{\mathrm{ADD}}_{(a,t)}], \quad (1)$$

where $c^{\mathrm{MC}}_{(a,t)}$ is the Channel Quality Indicator (CQI) of area a at TS t, $\eta(\cdot)$ is the spectral efficiency, α is a parameter < 1 to take into account protocols overhead, $\lambda^{\mathrm{BASE}}_{(a,t)}$ is the baseline bandwidth, $\lambda^{\mathrm{ADD}}_{(a,t)}$ is the additional amount of bandwidth redistributed by MC to area a. When the area is served by a UAV-SC, the throughput is expressed as:

$$R_{(a,t)} = \alpha \cdot \eta(c^{\mathrm{UAV}}_{(a,t)}) \cdot \lambda^{\mathrm{UAV}}_{(a,t)}, \quad (2)$$

where $c^{\mathrm{UAV}}_{(a,t)}$ is the CQI measured in the area when served by UAV-SC, and $\lambda^{\mathrm{UAV}}_{(a,t)}$ is the amount of bandwidth served by UAV-SC to the area. Clearly, in a real-world scenario, more complex resources, like Resource Blocks (RBs), are managed by RRM. Nevertheless, our assumption allows us to easily map the amount of assigned bandwidth of each area during a TS as a set of assigned RBs, a task that is deferred to the post-processing phase. Finally, we stress that, by moving the UAV-SCs over the territory, we are able to: (i) provide $\lambda^{\mathrm{UAV}}_{(a,t)}$ of bandwidth to areas covered by UAV-SC, and (ii) control the $\lambda^{\mathrm{ADD}}_{(a,t)}$ term to areas not covered by UAV-SC.

D. UAV-SC FEATURES

When a UAV-SC covers an area, this task needs to be planned inside the UAV mission, a procedure that typically requires multiple TSs. In this work, we assume that a UAV-SC performs one of the following actions in each TS: (i) *staying*, when the UAV-SC is parked at the ground site in a stand-by mode, (ii) *moving*, when the UAV-SC is flying but not covering an area (e.g., moving from ground site to a target area, or vice versa), (iii) *covering*, when the UAV-SC is flying and covering an area, and (iv) *recharging*, when the UAV-SC is parked at the ground site for recharging.

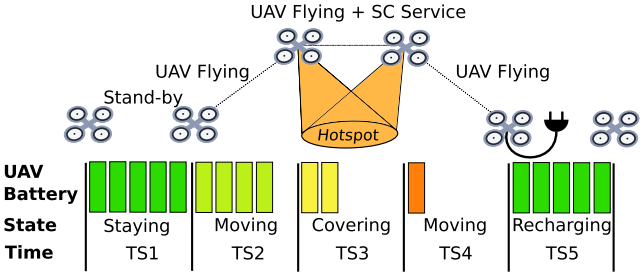

FIGURE 2. A typical mission for one unmanned aerial vehicle - small cell (UAV-SC) across a set of time slots (TSs).

Fig. 2 is an example of a UAV-SC mission across a set of TSs. During TS1, the UAV-SC is stationary, and its battery is at the maximum level. In the following TS, the moving state is set, the UAV-SC starts to fly and the required energy is drained from the battery. During TS3, the covering state

is set, and the UAV-SC provides the mobile service over an area. Clearly, the amount of energy consumed in this state is higher compared to the moving state, as the UAV-SC needs to activate SC radio functionalities to cover the area. During TS4, the UAV-SC flies back to the ground site. Clearly, in each TS, the amount of residual battery needs to be higher than a minimum level, to ensure a safe return to the ground site. At last, during TS5, the UAV-SC is recharged (recharging state in the figure), and it is able to perform a new mission once it is fully recharged. Overall, the considered mission requires five TSs to be completed. This aspect introduces a key feature of our model, which is the scheduling of UAV-SC missions (and their trajectories) over a set of multiple TSs, in order to improve $R_{(a,t)}$.

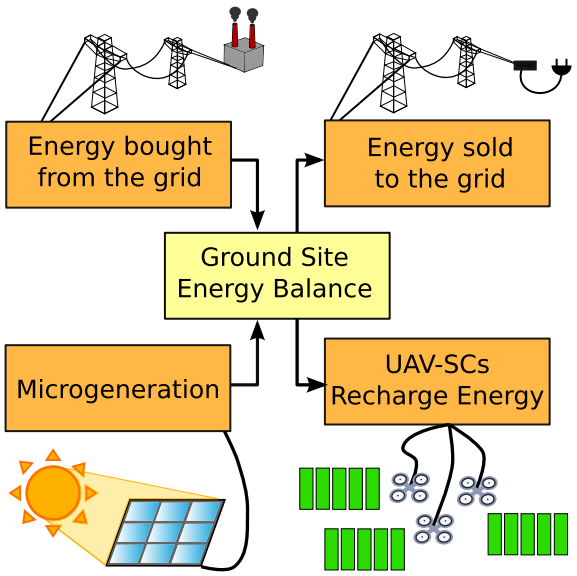

FIGURE 3. Grid-connected micro-generation (GMG) energy balance at ground site.

E. GMG FEATURES

A ground site provides recharging capabilities through GMG. In each TS, the ground site ensures that an optimal GMG energy balance is achieved – see Fig. 3. The ground site can be: (i) a consumer, when energy to recharge UAV-SCs is purchased entirely from the grid, (ii) a producer, when excess energy (from microgeneration) is sold to the electricity operator, (iii) a transparent player, when energy from microgeneration is used to recharge UAV-SCs, and (iv) a combination of cases (i) and (iii) or cases (ii) and (iii). Finally, we consider a set of solar panels as renewable energy sources for GMG.

IV. PROBLEM FORMULATION

We consider the management of a UAV-based mobile network that is comprised of a single MC and a set of UAV-SCs U deployed to cover a set of areas A over a time horizon that is decomposed into a set of time slots T of equal duration. We also define the set of places P as the union of the MC and the set of areas A (i.e., $P = \{\text{MC}\} \cup A$).

The UAV-SCs actions are modeled through a multi-period directed graph $G(N, L)$. The set of nodes N includes one node (p, t) for each place $p \in P$ and each time slot $t \in T$. The set of links L models the possible actions of any UAV-SC. Each link $l \in L$ is denoted as $[(p_1, t_1), (p_2, t_2)]$, where $t(l) = (p_1, t_1)$ and $h(l) = (p_2, t_2)$ are the tail and head of the link, respectively. Moreover, each link has a weight E_l, representing the amount of energy gained or consumed for the action. L is the union of four disjoint sets:

1) L^{MOV} modeling movements between two places $p_1, p_2 \in P$ (either from an area to MC or from MC to an area) - consumes energy $E^{\text{MOV}}_{p_1,p_2}$;
2) L^{STAY} modeling a UAV-SC staying in the MC - consumes zero energy;
3) L^{COV} modeling a UAV-SC coverage over an area $a \in A$ - consumes energy E^{COV}_a;
4) L^{REC} modeling a UAV-SC recharge in MC - increases energy E^{REC} for the UAV-SC, and consumes energy E^{REC} for the MC.

Consequently, it holds that: $L = L^{\text{MOV}} \cup L^{\text{STAY}} \cup L^{\text{COV}} \cup L^{\text{REC}}$.

We then introduce the following decision variables:

1) binary flow variables $f_{(l,u)}$ $\forall l \in L, u \in U$ - each variable equals 1 if UAV-SC u uses link l, executing the corresponding action, and 0 otherwise;
2) binary coverage variables $x_{(a,t)}$ $\forall a \in A, t \in T$ - each variable equals 1 if area a is covered by a UAV-SC in TS t, and 0 otherwise;
3) non-negative continuous variables $b_{(u,t)}$ $\forall u \in U$, $t \in T$ - each variable represents the battery level of UAV-SC u at TS t;
4) non-negative continuous variables E^{BUY}_t $\forall t \in T$ - each variable represents the amount of energy bought from the grid at TS t;
5) non-negative continuous variables E^{SELL}_t $\forall t \in T$ - each variable represents the amount of energy sold to the grid at TS t;
6) non-negative continuous variables $g^t_{(a,\text{MC})}$, $\forall a \in A$, $t \in T$ - each variable represents the fraction of bandwidth released by area a to the MC at TS t;
7) non-negative continuous variables $g^t_{(\text{MC},a)}$, $\forall a \in A$, $t \in T$ - each variable represents the fraction of additional MC bandwidth assigned to area a at TS t;
8) non-negative continuous variables γ^t $\forall t \in T$ - each variable represents the fraction of additional MC bandwidth available at TS $t \in T$ and not assigned to any area in TS t;
9) non-negative continuous variables $R^{\text{TOT}}_{(a,t)}$ $\forall a \in A$, $t \in T$ - each variable represents the downlink throughput of area a in TS t.

A. FEASIBILITY CONSTRAINTS

In order to model the actions of UAV-SCs, we rely on a flow model defined over the multi-period graph $G(N, L)$. We refer the reader to [27] for an exhaustive introduction to flow optimization in graphs. Specifically, we need one flow conservation constraint for each node (p, t) defined for each place $p \in P$ and TS $t \in T$, which enforces the coherence of

flows moving through the graph;

$$\sum_{\substack{l\in L:\\ h(l)=(p,t)}} f_{(l,u)} - \sum_{\substack{l\in L:\\ t(l)=(p,t)}} f_{(l,u)} = \beta^u_{(p,t)} \quad \forall p \in P, u \in U, t \in T \tag{3}$$

Here, $\beta^u_{(p,t)}$ is the flow balance for UAV-SC u in node (p,t). The value of $\beta^u_{(p,t)}$ is 0 for all nodes (p,t) with $t \geq 1$ (i.e., the flow must traverse the node). Instead, for the initial TS $t = 1$, $\beta^u_{(p,t)}$ is 0 for all areas (i.e., for $p \in A$) and -1 for $p = \{\text{MC}\}$, meaning that all the flow crossing the graph exits from node (MC, 1).[2] Moreover, to complete the flow model, we need to define one dummy node ω that is added to the set node N as sink node that must receive all flows. We also need to add a set of dummy links that connect the last period nodes to ω, i.e. we add one link from every node $(p, |T|)$ with $p \in P$ to the dummy node ω with null weight. The flow balance value β^u_ω for the sink node for each UAV-SC is equal to 1.

We then include the constraints to link area coverage variables to the value of appropriate subset of flow variables:

$$\sum_{u\in U} \sum_{l\in L^{\text{COV}}: h(l)=(a,t)} f_{(l,u)} \leq x_{(a,t)} \quad \forall a \in A, t \in T : t \geq 1 \tag{4}$$

Here, we impose that the coverage variable of a place p can be activated in a TS t *iff* one of the flow variables corresponding to coverage links of p is activated for some UAV-SC u.

We then impose the GMG energy balance in each TS through the following constraint:

$$\sum_{u\in U} E_l \cdot f_{(l,u)} = E^{\text{GMG}}_t + E^{\text{BUY}}_t - E^{\text{SELL}}_t \quad \forall l \in L^{\text{REC}} : h(l) = (\text{MC}, t) \wedge t(l) = (\text{MC}, t-1), t \in T \tag{5}$$

In particular, the total amount of energy requested to recharge the UAV-SCs (which appears in the left-hand-side of the equality as the product of the flow variables and the corresponding energy weights) must equal the summation of the locally produced energy E^{GMG}_t plus the energy bought from the grid E^{BUY}_t, minus the energy sold to the grid E^{SELL}_t.

In the following, we include the constraints related to the battery $b_{(u,t)}$ of each UAV-SC. Specifically, the UAV-SC battery level balance is expressed by:

$$b_{(u,t)} \leq b_{(u,t-1)} + \sum_{\substack{l\in L^{\text{MOV}}\cup L^{\text{REC}}\cup L^{\text{COV}}:\\ t(l)=(*,t-1)\\ h(l)=(*,t)}} E_l \cdot f_{(l,u)} \quad \forall u \in U, t \in T \tag{6}$$

that links the value of the battery level variables $b_{(u,t)}$ for each UAV-SC u between consecutive TSs, taking into account the battery variations due to actions of the UAV expressed through the flow variables.

[2]From the application point of view, this means that each UAV-SC $u \in U$ starts its actions from the MC.

Moreover, the battery level $b_{(u,t)}$ must be higher than a minimum level B^{MIN} and lower than a maximum level B^{MAX}, namely:

$$B^{\text{MIN}} \leq b_{(u,t)} \leq B^{\text{MAX}} \quad \forall u \in U, t \in T \tag{7}$$

We then focus on the computation of the bandwidth fraction $g^t_{(a,\text{MC})}$ that is released to the MC from every area $a \in A$ covered by a UAV-SC in each TS t. $g^t_{(a,\text{MC})}$ is computed as:

$$g^t_{(a,\text{MC})} = \frac{\lambda^{\text{BASE}}_{(a,t)}}{\lambda^{\text{TOT}}} \cdot x_{(a,t)} \quad \forall a \in A, t \in T \tag{8}$$

Specifically, the value of the variable $g^t_{(a,\text{MC})}$ is set equal to the value of the coverage variable $x_{(a,t)}$ multiplied by the fraction of bandwidth released to the MC, expressed as the ratio of baseline bandwidth $\lambda^{\text{BASE}}_{(a,t)}$ (previously introduced in Eq. (1)) and total bandwidth assigned to the areas λ^{TOT}.

We then need a set of constraints to express the fact that the additional bandwidth $g^t_{(\text{MC},a)}$ can be granted to an area a in t if and only if a is not covered by any UAV-SC at t. More formally, we have:

$$g^t_{(\text{MC},a)} \leq (1 - x_{(a,t)}) \quad \forall a \in A, t \in T \tag{9}$$

Moreover, we include the bandwidth conservation constraint at the MC side in each TS:

$$\sum_{a\in A} g^t_{(a,\text{MC})} = \sum_{a\in A} g^t_{(\text{MC},a)} + \gamma^t \quad \forall t \in T \tag{10}$$

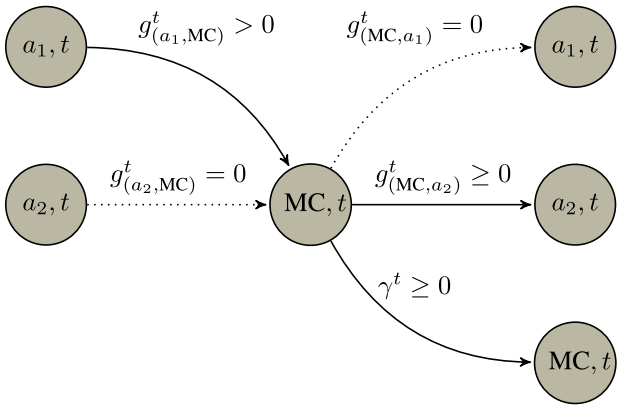

FIGURE 4. Example of macro cell (MC) bandwidth management.

The previous constraint ensures that the total bandwidth released by covering areas through UAV-SCs (which is modeled as the summation of the variables $g^t_{(a,\text{MC})}$ over all areas) must be equal to: i) the total additional bandwidth granted to areas not covered by UAV-SCs (which is modeled as the summation of the variables $g^t_{(\text{MC},a)}$ over all areas), plus ii) the fraction of bandwidth γ^t that is released directly to the MC and not granted to any area. Fig. 4 reports a simple example showing how constraints (8), (9) and (10) work in practice. In this example, we consider two areas, namely a_1 and a_2. At TS t area a_1 is covered by a UAV-SC, while area a_2 is served by the MC. Hence, $x_{(a_1,t)} = 1$, $x_{(a_2,t)} = 0$. According to constraint (8), (9) and (10), it holds that: $g^t_{(a_1,\text{MC})} > 0$,

$g^t_{(a_2,\mathrm{MC})} = 0$, $g^t_{(\mathrm{MC},a_1)} = 0$, $g^t_{(\mathrm{MC},a_2)} \geq 0$, $g^t_{(a_1,\mathrm{MC})} = g^t_{(\mathrm{MC},a_2)} + \gamma^t$.

Finally, we compute the total throughput $R^{\mathrm{TOT}}_{(a,t)}$ of each area a in each TS t by considering Eq. (1) and Eq. (2). More formally, we have:

$$R^{\mathrm{TOT}}_{(a,t)} = \alpha \cdot \{\underbrace{\eta(c^{\mathrm{UAV}}_{(a,t)}) \cdot \lambda^{\mathrm{UAV}}_{(a,t)} \cdot x_{(a,t)}}_{\text{UAV-SC Coverage Case}} + \underbrace{\eta(c^{\mathrm{MC}}_{(a,t)}) \cdot [\lambda^{\mathrm{BASE}}_{(a,t)} \cdot (1 - x_{(a,t)}) + \lambda^{\mathrm{TOT}} \cdot g^t_{(\mathrm{MC},a)}]}_{\text{MC Coverage Case}}\} \quad \forall a \in A, t \in T \qquad (11)$$

Specifically, when $x_{(a,t)} = 1$, a is covered by a UAV-SC and the throughput is provided by the UAV-SC term. Instead, when $x_{(a,t)} = 0$, the area is not covered by a UAV-SC and the throughput is derived from the MC.

B. COMPLETE OPTIMIZATION MODEL.

The overall MaxUAVProfit model is completed by including the following objective function:

$$\max \sum_{t \in T} \left(\underbrace{\pi \sum_{a \in A} R^{\mathrm{TOT}}_{(a,t)}}_{\text{Throughput Revenue}} + \underbrace{C^{\mathrm{SELL}}_t E^{\mathrm{SELL}}_t}_{\text{Energy Revenue}} - \underbrace{C^{\mathrm{BUY}}_t E^{\mathrm{BUY}}_t}_{\text{Energy Cost}} \right) \qquad (12)$$

which pursues the profit maximization by summing over all TSs: i) the revenue from the throughput of the areas (expressed as the total throughput $\sum_{a \in A} R^{\mathrm{TOT}}_{(a,t)}$ multiplied by the unitary throughput revenue π), ii) the total revenue from selling energy to the grid (where C^{SELL}_t is the unitary selling price in TS $t \in T$) and iii) the total cost for buying energy from the grid (where C^{BUY}_t is the unitary buying price in TS $t \in T$).

Subject to the constraints:

UAV-SC flow conservation constraint:	Eq. (3)	
UAV-SC coverage activation constraint:	Eq. (4)	
GMG energy balance constraint:	Eq. (5)	
UAV-SC battery balance constraint:	Eq. (6)	
UAV-SC battery bounds:	Eq. (7)	(13)
Bandwidth release computation:	Eq. (8)	
Additional bandwidth constraint:	Eq. (9)	
Bandwidth conservation constraint:	Eq. (10)	
Computation of the area throughput:	Eq. (11)	

under variables: $f_{(l,u)} \in \{0, 1\}$, $x_{(a,t)} \in \{0, 1\}$, $b_{(u,t)} \geq 0$, $E^{\mathrm{BUY}}_t \geq 0$, $E^{\mathrm{SELL}}_t \geq 0$, $g^t_{(a,\mathrm{MC})} \geq 0$, $g^t_{(\mathrm{MC},a)} \geq 0$, $\gamma^t \geq 0$, $R^{\mathrm{TOT}}_{(a,t)} \geq 0$.

V. SCENARIO DESCRIPTION

We divide the description of the scenarios in the following subsections: i) areas, MC and TSs (Sec. V-A), ii) UAV-SC energy consumption (Sec. V-B), ii) GMG energy components (Sec. V-C).

FIGURE 5. Torrino-MezzoCammino terrain view including: Measurement points (bordeaux pins), center of the areas (blue pins) and macro cell (MC) position (yellow pin).

A. AREAS, MACRO CELL AND TIME SLOTS

We consider a set A including 10 areas (i.e., $|A| = 10$) and one MC located in the Torrino-MezzoCammino neighborhood (Rome, Italy), a zone populated by more than 10000 inhabitants. Fig. 5 reports a terrain view with the positioning of the centers of the area and the MC. In order to obtain realistic information about the CQI values in each area ($c^{\mathrm{MC}}_{(a,t)}$), we perform a measurement campaign, by exploiting the CellMapper app, which is installed on a Samsung S6 Edge smartphone with a Vodafone sim card. CellMapper allows to obtain raw data from a cellular network, which include the ID of the serving BS, the BS frequency band, as well as the CQI measured at current location. In our work, we consider a set of measurement points inside the coverage area of the MC. The locations of the measurements are shown with bordeaux pins in Fig. 5. For each location, we measure the average CQI over a time window of 3 minutes, during a working day of the week. During this process, we make sure that the BS ID is the one of the selected MC, as we assume that the set of areas A is covered by one MC.[3] In addition, we check that the smartphone is connected through 4G connectivity. In the following, we collect the CQI measurements, and we compute the average CQI $c^{\mathrm{MC}}_{(a,t)}$ for each area, by considering all the measurements in a radius of 150 [m] from the center of the area.[4] Tab. 1 (second column) reports the average CQI values for each area. As expected, the area CQI is in general lower than the maximum one, due to the fact that:

[3]The extension of our work to the case in which multiple MCs serve the same area is left for future work.

[4]This value can be representative of the coverage for one SC, as well as of the size for one hotspot. Moreover, it guarantees no overlap among the different areas.

TABLE 1. Channel quality indicator (CQI) and spectral efficiency values for each area served by the macro cell (MC).

Area ID	CQI ($c^{MC}_{(a,t)}$)	Spectral efficiency ($\eta(c^{MC}_{(a,t)})$)
1	6	0.822 [bps/Hz]
2	7	1.033 [bps/Hz]
3	5.8	0.770 [bps/Hz]
4	6.6	0.943 [bps/Hz]
5	10.6	2.146 [bps/Hz]
6	8	1.339 [bps/Hz]
7	11	2.322 [bps/Hz]
8	8.3	1.454 [bps/Hz]
9	10	1.911 [bps/Hz]
10	11.2	2.403 [bps/Hz]

i) different areas are far from the serving MC, and ii) Non Line of Sight (NLOS) conditions w.r.t. the MC dominate the measurements. Given each measured CQI value $c^{MC}_{(a,t)}$, we then adopt the CQI-spectral efficiency conversion of [28] to retrieve $\eta(c^{MC}_{(a,t)})$.[5] The resulting values are reported in Tab. 1 (third column).

Focusing on the UAV-SC, we assume $c^{UAV}_{(a,t)} = 15$. This assumption, although optimistic at a first glance, allows evaluating the maximum gain achievable when the UAV-SC is serving an area. In addition, the relatively high CQI value provided by the UAV-SC is also motivated by the fact that users in the area may globally experience short distance from the serving UAV-SC, as well as Line Of Sight (LOS) conditions. Consequently, a CQI value higher than the one measured when the area is served by the MC may be observed. Similarly to the MC case, we adopt the values in [28] to compute $\eta(c^{UAV}_{(a,t)})$, which is equal to 3.883 [bps/Hz].

Focusing then on the bandwidth features, the MC currently serving the Torrino-Mezzocammino area exploits the 1800 [MHz] frequency with a 20 [MHz] bandwidth. We then set the total bandwidth assigned to the areas λ^{TOT} as the ratio between the size of all the areas and the MC coverage over Torrino-Mezzocammino, resulting in $\lambda^{TOT} = 7.18$ [MHz]. We then assume that λ^{TOT} is equally split among the areas, thus obtaining $\lambda^{BASE}_{(a,t)} = 0.718$ [MHz] $\forall a \in A, t \in T$. On the other hand, UAV-SC provides an amount of bandwidth exclusively reserved to an area (i.e, separated from the bandwidth of the MC). In particular, we set $\lambda^{UAV}_{(a,t)} = 5$ [MHz] $\forall a \in A, t \in T$, a typical SC setting. Moreover, we set $\alpha = 0.64$ [28].

Finally, we consider a set of TSs T over a 24h period, with a TS duration $\Delta(t)$ of 600 [s]. In this way, we are able to control the UAV-SC actions and the GMG energy balance in a short time scale, while still allowing the solution of the problem instance on a server machine. Without loss of generality, we also assume that the CQI values are constant over the considered TS period.[6]

B. UAV-SC ENERGY CONSUMPTION

We then compute the energy consumed by each UAV-SC, starting from the detailed consumption model of [4], [29] to properly take into account the energy components when the UAV-SC performs the different actions. Clearly, we expect that the COV action has the largest contribution to energy (due to the fact the UAV-SC hovers over an area). However, in our work we consider also other actions, like moving from a site to an area. This fact, coupled with the need of precisely estimating the UAV-SC energy consumption, stimulated us to employ a detailed energy consumption model.

In general, the total UAV-SC energy consumption for each link l of the multi-period directed graph $G(N, L)$ is the composition of the following terms: i) level flight energy consumption $E_F(l)$; ii) vertical flight energy consumption $E_V(l)$; iii) blade drag profile energy consumption $E_B(l)$; iv) SC serving energy consumption $E_S(t)$. In the following, we briefly review each of the aforementioned terms. We refer the reader to [4], [29] for a detailed description of i)-iii).

1) LEVEL FLIGHT ENERGY CONSUMPTION

This term takes into account the horizontal contribution to the energy consumption, and it is spent when the UAV-SC is flying (i.e., COV and MOV actions). More formally, $E_F(l)$ is expressed as:

$$E_F(l) = \frac{(m \cdot g)^2}{\sqrt{2}\delta\sigma} \frac{1}{\sqrt{[V_H(l)]^2 + \sqrt{[V_H(l)]^4 + \left(\frac{m \cdot g}{\sigma}\right)^2}}} \Delta(t), \quad l \in L^{MOV} \cup L^{COV} \tag{14}$$

where m is the mass of the UAV-SC, g is the gravitational acceleration, δ is the air density, σ is the area of the UAV rotor disks, $V_H(l)$ is the horizontal speed, which is computed as:

$$V_H(l) = \frac{\epsilon(p_1, p_2)}{\Delta(t)} \tag{15}$$

where $\epsilon(p_1, p_2)$ is the distance between place p_1 and place p_2, and $\Delta(t)$ is the TS duration.

By observing in more detail Eq. (14), the higher is $V_H(l)$, the lower is $E_F(l)$ (by assuming all the other parameters fixed). This is an expected result, since the air flow increases the lift of the UAV-SC. Moreover, when m is increased, the level flight energy consumption $E_F(l)$ is also increased, due to the fact that more energy is required to keep flying the UAV-SC (as expected). Eventually, the increase of the rotor disk area σ tends to decrease $E_F(l)$, due to the fact that the lift provided by the air flow can be better exploited by a larger rotor disk size. Finally, the decrease of the TS duration $\Delta(t)$ may also result in a decrease of $E_F(l)$. However, since this decrease has also an impact on the horizontal speed $V_H(l)$ term of Eq.(15), the TS duration needs to be carefully evaluated w.r.t. the maximum horizontal speed supported by the UAV-SC.

In our problem, we set $m = 12$ [kg] (i.e, we assume that the total weight of the UAV and the SC is not negligible), $g = 9.81$ m/s^2, $\delta = 1.225$ kg/m^3 [4], $\sigma = 3.141$ [m^2] (i.e., we assume a diameter of 2 [m] for the rotor disk, and hence a pretty big UAV-SC), $\epsilon(p_1, p_2)$ in accordance to the

[5] For non-integer values, we compute the weighted average between the lower and higher integer values.

[6] The actual CQI values may vary as the number of users and/or their traffic requests are changed over time. The investigation of this aspect is left for future work.

real positions in the scenario of Fig. 5. Moreover, we assume that $V_H(l) = 0, \quad \forall l \in L^{\text{COV}}$, i.e., when the UAV-SC is covering an area, it is kept above the center of the area. In this condition, $E_F(l)$ assumes a non zero value, due to the presence of the non-zero terms m, g, δ, σ in Eq. (14).

2) VERTICAL FLIGHT ENERGY CONSUMPTION

This term takes into account the contribution of energy when the UAV-SC is climbing/descending from/to a given height. More formally, we have:

$$E_V(l) = m \cdot g \cdot V_C(l) \cdot \Delta(t), \quad l \in L^{\text{MOV}} \tag{16}$$

where $V_C(l)$ is the vertical climbing/descending speed, which can be positive or negative, depending if the UAV-SC is climbing from the ground site to the center of an area, or descending from the center of an area to the ground site. More formally, we have the following expression:

$$V_C(l) = \begin{cases} \dfrac{\kappa}{\Delta(t)} & \text{if } l \in L^{\text{MOV}}, p_1 = \text{MC}, p_2 \in A, \\ -\dfrac{\kappa}{\Delta(t)} & \text{if } l \in L^{\text{MOV}}, p_1 \in A, p_2 = \text{MC}, \end{cases} \tag{17}$$

where $(p_1, t_1) = t(l)$, $(p_2, t_2) = h(l)$, $t_1 = (t-1)$, $t_2 = t$, κ is the height from ground, which is set to 200 [m] in our case. In this way, in fact, we expect that the UAV-SC is in LOS conditions w.r.t. the users in the served area.

In general, $E_V(l)$ is positive if the UAV-SC is climbing (negative if it is descending). Clearly, UAV-SCs with a given value of mass m will consume more energy compared to the ones with a smaller value of m. Moreover, the increase of the climbing speed $V_C(l)$ also results in an increase of $E_V(l)$. Eventually, we point out that $E_V(l)$ becomes negative when the UAV-SC is descending, due to the fact that UAV-SC flight has the same direction of the gravitational acceleration force. Finally, we point out that $E_V(l)$ is also proportional to the TS duration $\Delta(t)$. However, since the climbing speed $V_C(l)$ depends on $\Delta(t)$ (appearing also in Eq. (17)), the setting of the TS duration has to take into account the maximum vertical speed supported by the UAV-SC.

3) BLADE DRAG PROFILE ENERGY CONSUMPTION.

This term takes into account the air frictional resistance of the UAV-SC blades against the air, and it is expressed as:

$$E_D(l) = \frac{1}{8}\varphi \cdot \delta \cdot \sigma \cdot [V_H(l)]^3 \cdot \Delta(t), \quad l \in L^{\text{MOV}} \tag{18}$$

where φ is the drag profile coefficient, depending on the aerodynamic profile of the UAV-SC.

Clearly, when the UAV-SC is moving on the horizontal plane very fast, $E_D(l)$ is not negligible, since $V_H(l)$ appearing in Eq.(18) is multiplied by the power of three. Moreover, UAV-SCs with a large area of the rotor disks σ tend to consume more blade drag energy profile $E_D(l)$ compared to the ones with a small area.

In our scenario, we set φ to 0.08, in accordance to [4]. In addition, $E_D(l)$ is equal to 0 when the UAV-SC is covering, due to the fact that the UAV-SC hovers over an area. In this case, $V_H(l) = 0$ and consequently $E_D(l) = 0$. On the other hand, this term is larger than 0 when the UAV-SC is moving from/to an area.

4) SMALL CELL SERVING ENERGY CONSUMPTION.

This term takes into account the amount of energy that is consumed when the SC radio functionalities are activated. More formally, we have:

$$E_B(t) = P_B(t) \cdot \Delta(t), \quad \forall l \in L^{\text{COV}} \tag{19}$$

In the above equation, $P_B(t)$ denotes the SC power consumption for serving the users, set to 200 [W], in accordance to [30].[7]

In this work, we have assumed that the $E_B(t)$ term is activated when the UAV-SC covers an area. On the other hand, when the UAV-SC is moving from/to an area the SC is turned off and $E_B(t) = 0$.

5) OVERALL UAV-SC ENERGY MODEL.

Finally, we summarize the mapping of the energy different components to each UAV-SC action (i.e., MOV, COV, REC, STAY). In particular, it holds that $E^{\text{MOV}}_{p_1,p_2} = E_F(l) + E_V(l) + E_D(l), \forall p_1, p_2 \in P, \forall l \in L^{\text{MOV}} : h(l) = (p_2, t_2), t(l) = (p_1, t_1)$ and $E^{\text{COV}}_a = E_F(l) + E_B(t), \quad \forall a \in A, \forall l \in L^{\text{COV}} : h(l) = (a, t_2), t(l) = (a, t_1)$. Eventually, we set $E^{REC} = 1000$ [Wh], $E^{\text{STAY}} = 0$, $B^{\text{MIN}} = 100$ [Wh], $B^{\text{MAX}} = 1000$ [Wh] in accordance to [3].

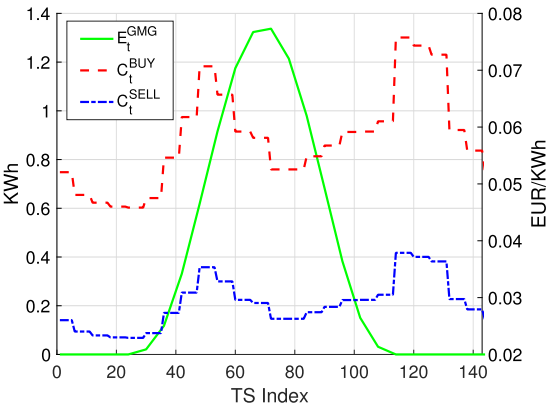

FIGURE 6. Grid-connected MicroGeneration (GMG) vs. time E_t^{GMG}, cost of energy bought from the grid vs. time C_t^{BUY}, cost of energy sold to the grid vs. time C_t^{SELL}.

C. GMG ENERGY COMPONENTS

We set E_t^{GMG} by assuming a solar panel generation system of 10 [kWp] of power. The values of E_t^{GMG} are then extracted from the PVWatts calculator [31], by considering the features of the location (e.g., sun irradiation) and a day during the month of May. Fig. 6 reports the trend of E_t^{GMG} vs. time. More in depth, the production of solar panel energy is higher during the day (central part of the plot) and zero during the

[7]The integration of more detailed SC power consumption models is left for future work.

night (side parts of the plot). In addition, the figure reports also the values of C_t^{BUY} and C_t^{SELL}, which are taken from the Italian electricity market [32], again during the same month of E_t^{GMG} values. Clearly, it holds that $C_t^{\text{BUY}} \geq C_t^{\text{SELL}}$, $\forall t \in T$. Moreover, we can observe that both C_t^{BUY} and C_t^{SELL} vary over time, with two peaks during late morning and late evening.

VI. FINDINGS

We then run the MaxUAVProfit problem on the considered scenario. We include the following strategies for comparison:

- OptGMG: max $\sum_{t\in T}(C_t^{\text{SELL}}E_t^{\text{SELL}} - C_t^{\text{BUY}}E_t^{\text{BUY}})$, s.t. Eq. (3)-Eq. (11). The goal of this strategy is to maximize the energy sold and to minimize the energy purchased. Since the area throughput is not included in the objective function, this problem always keeps the UAV-SCs in the STAY state;
- OptT: max $\sum_{a\in A}\sum_{t\in T} R_{(a,t)}^{\text{TOT}}$, s.t. Eq. (3)-Eq. (11). The goal of OptT is to maximize the throughput, without considering the impact on the energy sold and/or purchased;
- MaxCov: max $\sum_{p\in A}\sum_{t\in T} x_{(p,t)}$ s.t. Eq. (3)-Eq. (11). This formulation (whose simplified version is presented in [3]) maximizes the number of areas covered by the UAV-SCs, without considering the contribution in terms of area throughput and/or energy purchased/sold.

The strategies are coded on CPLEX (v.12.7.1) and executed on a Dell EMC PowerEdge 230 Server with 64 [GB] of RAM and four Intel Xeon E3-1230v6 CPU at 3.5 [GHz]. Unless otherwise specified, we introduce the following CPLEX settings: i) maximum time limit equal to 86400 [s], ii) minimum gap of 1%, and iii) polishing option activated after 90 [s].

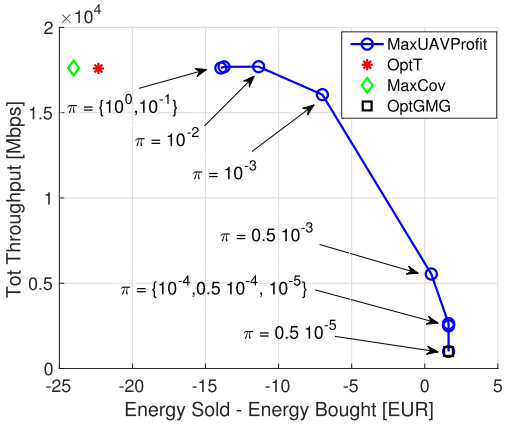

FIGURE 7. Pareto frontier of MaxUAVProfit strategy. The findings of OPTGMG, OPTT, MaxCov formulations are also highlighted.

We initially explore the impact of varying the parameter π, which governs the weight of the area throughput w.r.t. the energy costs/profits. Clearly, since maximizing the area throughput and optimizing the GMG energy are two competing objectives, the variation of π allows one to derive the Pareto frontier of the MaxUAVProfit problem. Fig. 7 reports the Pareto frontier considering the total area throughput on the y-axis and the term $\sum_{t\in T}(C_t^{\text{SELL}}E_t^{\text{SELL}} - C_t^{\text{BUY}}E_t^{\text{BUY}})$ on the x-axis. The figure also reports the positioning of OptGMG, OptT and MaxCov strategies. By varying π, MaxUAVProfit moves on the Pareto frontier, and achieve solutions that are able to leverage the tradeoff between GMG energy components and throughput. This is a great advantage compared to the other solutions. For example, the OptGMG strategy provides a positive term in terms of GMG profit, but this policy has a negative impact on the throughput, which is notably reduced compared to the other strategies. On the other hand, both OptT and MaxCov are able to maximize the throughput, but the obtained GMG costs are not negligible. Our solution is instead able to leverage the GMG energy/throughput trade off, which can be governed by the operator through the setting of the π parameter..

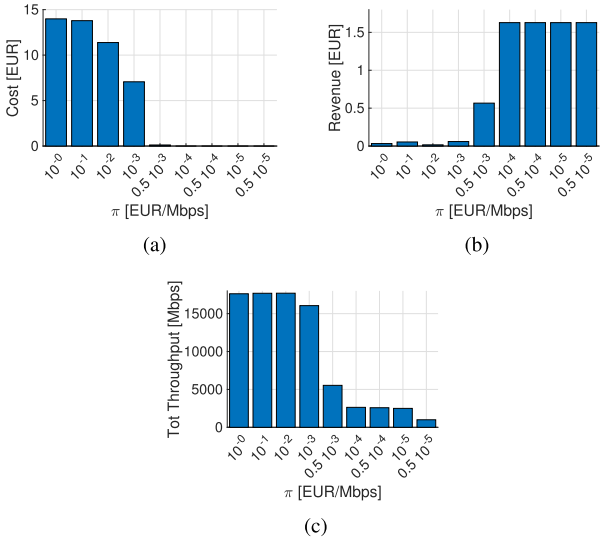

FIGURE 8. Breakdown of the components of the objective function vs. the variation of the π parameter (MaxUAVProfit strategy). (a) Total cost for the energy bought from the grid. (b) Total revenue for the energy sold to the grid. (c) Total throughput.

In the following, we investigate in more detail the impact of π variation on the different terms appearing in the objective function of MaxUAVProfit. Fig. 8 reports the breakdown in terms of: i) total cost for energy bought (Fig. 8(a)), ii) total revenue from energy sold (Fig. 8(b)), and iii) total throughput (Fig. 8(c)). Interestingly, the total costs from the energy bought and the total revenue from the energy sold are characterized by opposite trends. In particular, the cost of energy bought passes from around 14 [EUR] to 0 [EUR] when π is decreased. On the other hand, the total revenue for the energy sold passes from almost zero values to more than 1.5 [EUR]. Eventually, when the total cost for the energy bought is more than 6 [EUR] (Fig. 8(a)), the energy sold is almost negligible (Fig. 8(b)). This event occurs when UAV-SCs are frequently used to serve the areas. Hence, a large amount of energy is derived from the grid and from microgeneration. Consequently, little (or none) energy is sold to the grid. Note that the lower cost per unit of energy that is sold w.r.t. those bought (Fig. 6) guarantees that the profit is realized by selling

locally produced energy to the grid (in other words, there is no gain for the operator to buy energy from the grid and sell this energy back to the grid). Clearly, the cost/revenues shown here are obtained for a system composed of one ground site, on a daily basis. By scaling these numbers to a larger portion of territory (e.g., composed of thousands of ground sites), as well as by considering a yearly horizon, it is possible to predict a 1,000,000-fold increase of these values; thus, impacting the operator's OPerating EXpenditures (OPEX).

Focusing then on the throughput (Fig. 8(c)), this metric passes from more than 15000 [Mbps] when $\pi = 1$ to less than 1000 [Mbps] when $\pi = 0.5 \cdot 10^{-5}$, thus experiencing a variation of more than one order of magnitude. In addition, even if the presented results are referred to the set of areas and not to the users, we may expect a similar improvement when a single user is take into account. Actually, the boost in the throughput is realized when UAV-SCs cover the selected areas, and it is a combination of the following aspects: i) the improvement in CQI values for the areas covered by UAV-SCs, ii) the fact that each UAV-SC offers an amount of bandwidth, which is separated from the MC one, and it is allocated to serve a specific area, iii) the amount of bandwidth released from areas covered by UAV-SCs, which becomes available to other areas, not covered by UAV-SCs.

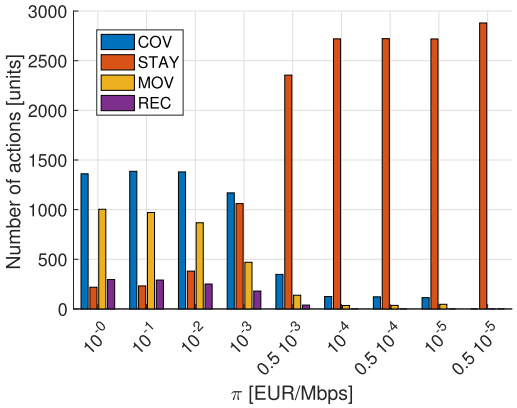

FIGURE 9. Adopted actions by Unmanned aerial vehicles - small cells (UAV-SCs) vs. variation of π parameter (MaxUAVProfit strategy).

We now focus on the different actions taken by UAV-SCs. Fig. 9 reports the breakdown of cumulative actions set by the MaxUAVProfit formulation, again for different values of π. As expected, when the throughput is at its maximum (left part of the figure), UAV-SCs are frequently used, being the COV, MOV and REC actions frequently set. When $\pi \geq 10^{-3}$ (center part of the figure), the STAY is frequently imposed. Moreover, when $10^{-4} \leq \pi \leq 10^{-5}$ (right part of the figure), UAV-SCs only use the amount of initial battery to perform some (few) COV and MOV actions, due to the fact that GMG energy components become predominant w.r.t. throughput. Finally, when $\pi = 0.5 \cdot 10^{-5}$, UAV-SCs are always in the STAY state. Similarly to the OptGMG strategy, in this case there is not financial incentive for the operator to serve the areas with the UAV-SCs.

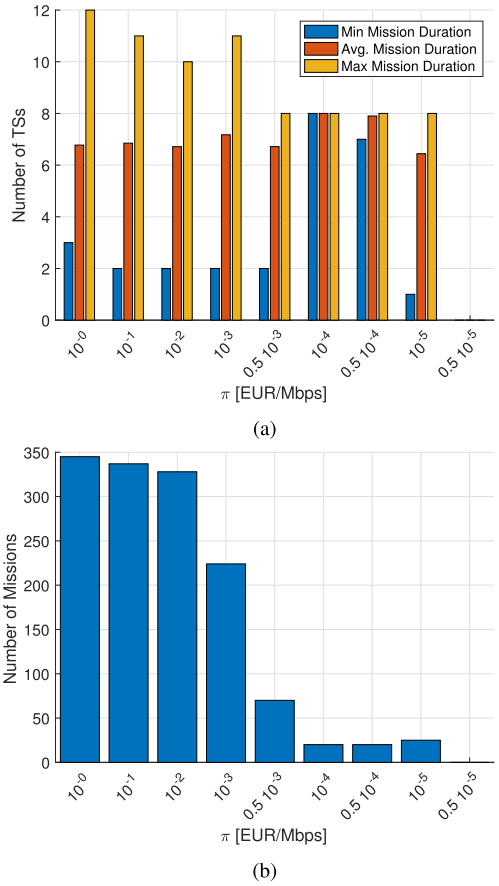

FIGURE 10. Unmanned aerial vehicles - small cells (UAV-SCs) mission duration and number of missions vs. variation of π parameter for the MaxUAVProfit strategy. (a) Mission duration. (b) Number of missions.

In the following, we focus on the missions that are performed by the UAV-SCs. We define a mission as a sequence of consecutive MOV/COV actions, starting from a MOV from a site to an area until: i) the UAV-SC returns back to a site with another MOV action, or ii) the current TS is the last one. Fig. 10 reports the obtained results in terms of: minimum, average and maximum mission duration (Fig. 10(a)) and total number of missions (Fig. 10(b)). Interestingly, when the UAV-SCs are used (left part of the subfigures), each mission lasts for different consecutive TSs. For example, when $\pi = 1$, the average duration of the UAV-SCs missions is around 7 TSs. However, as soon as π is decreased, both the maximum mission duration and the number of missions are notably reduced. At last, when $\pi = 0.5 \cdot 10^{-5}$, no UAV-SC is used. Consequently, both the minimum/average/maximum mission duration and the number of missions are equal to zero.

In the last part of our work, we focus on the amount of bandwidth released by UAV-covered areas, which becomes available to MC and can be used to improve services to other zones (not covered by the UAV-SCs). Fig. 11(a) reports the total number of events in which: i) some bandwidth is released from an area to MC (blue bars), ii) some MC bandwidth derived from i) is assigned to an area (light red bars). Note that case i) corresponds to counting variables

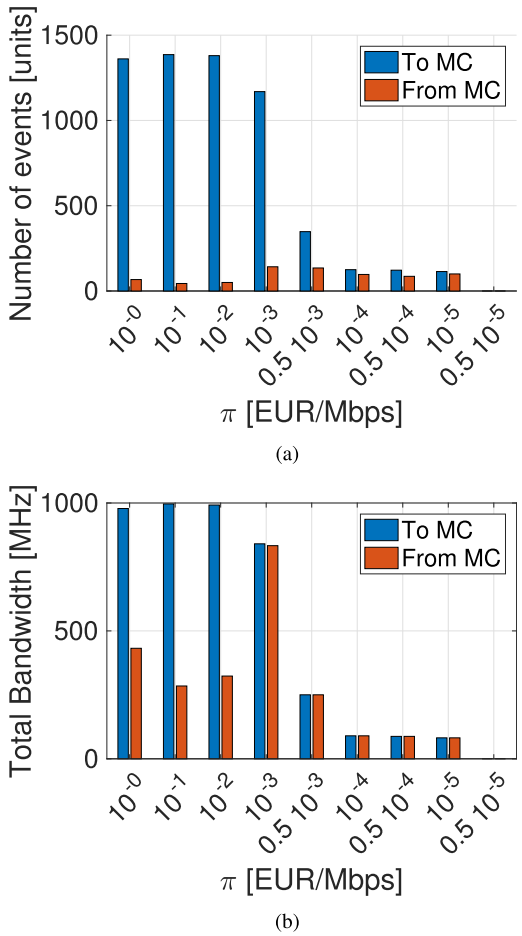

FIGURE 11. Resources released to macro cell (MC) by unmanned aerial vehicles - small cells (UAV-SCs) covered areas and assigned by MC to areas not covered by UAV-SCs (in addition to $\lambda_{(a,t)}^{BASE}$) vs. variation of π parameter (MaxUAVProfit strategy). (a) Number of events. (b) Bandwidth.

$g_{(a,\mathrm{MC})}^{t} > 0$, while case ii) is equivalent to counting variables $g_{(\mathrm{MC},a)}^{t} > 0$. By observing Fig. 11(a), we can note that the number of events during which the bandwidth is released to the MC tends to decrease as π is reduced, due to the fact that the UAV-SCs are less frequently exploited. On the other hand, the number of events during which the additional bandwidth is assigned by the MC is clearly lower compared to the previous event type. In addition, the trend reported in the figure is almost constant. At last, when $\pi = 0.5 \cdot 10^{-5}$, UAV-SCs are not used at all, and hence the number of events with released and/or assigned bandwidth becomes zero.

Finally, Fig. 11(b) reports the results in terms of released/assigned bandwidth, which is computed as $\sum_a \sum_t \lambda^{TOT} \cdot g_{(a,\mathrm{MC})}^{t}$ for case i) and $\sum_a \sum_t \lambda^{TOT} \cdot g_{(\mathrm{MC},a)}^{t}$ for case ii). In particular, the released bandwidth passes from around 1000 [MHz] when $\pi = 1$ to a zero value when $\pi = 0.5 \cdot 10^{-5}$. On the other hand, the assigned bandwidth presents a different trend: it is almost increasing when π is decreased up to 10^{-3}, then it is decreasing for lower values of π. Eventually, we observe that the bandwidth released by UAV-covered areas is redistributed by MC to cover (few) areas (not covered by the UAV-SCs). This choice appears to be very effective, as the relatively small contributions in terms of bandwidth are summed and focused on few zones. Moreover, as soon as the UAV-SCs are less frequently used (center part of the figure), all bandwidth released by covered areas tend to be redistributed to others. This is expected, as in these conditions the released bandwidth becomes a valuable resource for areas not covered by UAV-SCs. At last, when $\pi = 0.5 \cdot 10^{-5}$, UAV-SCs are not used, and hence no bandwidth is released to MC.

VII. DISCUSSION AND IMPLEMENTATION ISSUES

Our work assumes that UAV-SCs can fly over the territory. However, there may be legal barriers in deploying UAVs over populated areas. For example, in Italy, an authorization is requested in order to fly over zones with private houses. Nevertheless, UAVs are deployed for video surveillance purposes, even in the considered Torrino-MezzoCammino scenario (see e.g., [33]). In addition, we point out that a UAV-based architecture can be very effective in first responder search and rescue missions. To this aim, there are already efforts in deploying UAV-based systems in current environments. For example, the city of Chula Vista (CA) has recently launched a test program [34] to deploy UAVs for proactive public safety operations by the Chula Vista Police Department. In addition, there are also efforts to fund UAV-based research projects for response technologies. For example, the Department of Homeland Security Science and Technology Directorate has issued a request for innovators [35], seeking to prototype, test and transition cutting-edge emergency response technologies, including UAVs.

Another aspect that may impact the results is the type of UAV in use. In this work, we have considered a quadcopter-based UAVs deployment. However, we point out that other types of UAVs, like the wing-based ones, require a take-off/landing strip, which may be challenging to be deployed in an area including different buildings and/or obstacles. In addition, providing cellular connectivity by means of a SC mounted on a wing-based UAV introduces additional challenges, such as the need of taking into account the impact of UAV mobility during coverage, which may introduce strong variations to the wireless channel conditions between the UAV and the users. On the other hand, all these issues are avoided with quadcopter-based UAVs, which are able to easily take off/land on a vertical plane, as well as being capable to provide a cellular connectivity similar to a SC mounted on a fixed tower when hovering over an area. Certainly, quadcopter-based UAVs are less energy-efficient compared to wing-based ones. However, we have done our best to take into account a realistic UAV energy consumption model. Thus, we believe that the presented work is meaningful and useful also for future research activities, which may be tailored e.g. to the design of energy-efficient quadcopter UAVs.

VIII. CONCLUSIONS AND FUTURE WORK

In this paper, we studied the joint management of the throughput to a set of areas and the GMG energy of the

ground site. Specifically, we proposed the MaxUAVProfit model, designed to schedule UAV-SC missions over time, manage the amount of MC bandwidth consumption, control the throughput of users, and ensure the GMG energy balance. Findings from our evaluation (based on a realistic scenario) demonstrated that, by varying the value of the π parameter, MaxUAVProfit leverages the trade-off between GMG energy and area throughput, a key aspect not considered by competing policies. This is a clear advantage for the operator, who may then decide how to set π, depending on costs and performance needs. In addition, we have studied in detail the impact of π variation in terms of energy bought, energy sold, area throughput, UAV-SCs actions, UAV-SCs missions, assigned/released bandwidth events and total assigned/released bandwidth.

As future work, we plan to optimize the varying setting of π over time (e.g., by allowing throughput maximization during periods of high traffic, and GMG optimization during periods of low traffic). In addition, focusing on orchestration aspects is another potential research agenda. This includes the selection of the orchestrator to run the MaxUAVProfit model, as well as the communication between the orchestrator and the managed devices (e.g., UAV-SCs, MC, GMG components), which may include security issues. Eventually, more detailed aspects, like the variation of the CQI values over time, more detailed SC power consumption models, multiple MCs serving the same area, should be also studied. Finally, we plan also to design efficient algorithms to tackle the solution of the problem also for very large instances, e.g., by considering decentralized approaches.

REFERENCES

[1] Y. Zeng, R. Zhang, and T. J. Lim, "Wireless communications with unmanned aerial vehicles: Opportunities and challenges," *IEEE Commun. Mag.*, vol. 54, no. 5, pp. 36–42, May 2016.

[2] M. Mozaffari, W. Saad, M. Bennis, Y.-H. Nam, and M. Debbah, "A tutorial on UAVs for wireless networks: Applications, challenges, and open problems," *IEEE Commun. Surveys Tuts.*, to be published.

[3] L. Amorosi, L. Chiaraviglio, F. D'Andreagiovanni, and N. Blefari-Melazzi, "Energy-efficient mission planning of UAVs for 5G coverage in rural zones," in *Proc. IEEE Int. Conf. Environ. Eng. (EE)*, Mar. 2018, pp. 1–9.

[4] Y. Sun, D. Xu, D. W. K. Ng, L. Dai, and R. Schober, "Optimal 3D-trajectory design and resource allocation for solar-powered UAV communication systems," *IEEE Trans. Commun.*, to be published.

[5] A. Trotta, M. D. Felice, F. Montori, K. R. Chowdhury, and L. Bononi, "Joint coverage, connectivity, and charging strategies for distributed UAV networks," *IEEE Trans. Robot.*, vol. 34, no. 4, pp. 883–900, Aug. 2018.

[6] D. Infield and F. Li, "Integrating micro-generation into distribution systems—A review of recent research," in *Proc. IEEE Power Energy Soc. Gen. Meeting Convers. Del. Elect. Energy 21st Century*, Jul. 2008, pp. 1–4.

[7] S. Jeong, O. Simeone, and J. Kang, "Mobile edge computing via a UAV-mounted cloudlet: Optimization of bit allocation and path planning," *IEEE Trans. Veh. Technol.*, vol. 67, no. 3, pp. 2049–2063, Mar. 2018.

[8] J. Xu, Y. Zeng, and R. Zhang, "UAV-enabled wireless power transfer: Trajectory design and energy optimization," *IEEE Trans. Wireless Commun.*, vol. 17, no. 8, pp. 5092–5106, Aug. 2018.

[9] C. Lin, D. He, N. Kumar, K.-K. R. Choo, A. Vinel, and X. Huang, "Security and privacy for the Internet of drones: Challenges and solutions," *IEEE Commun. Mag.*, vol. 56, no. 1, pp. 64–69, Jan. 2018.

[10] J. Wu, S. Guo, H. Huang, W. Liu, and Y. Xiang, "Information and communications technologies for sustainable development goals: State-of-the-art, needs and perspectives," *IEEE Commun. Surveys Tuts.*, vol. 20, no. 3, pp. 2389–2406, 3rd quart., 2018.

[11] R. I. Bor-Yaliniz, A. El-Keyi, and H. Yanikomeroglu, "Efficient 3-D placement of an aerial base station in next generation cellular networks," in *Proc. IEEE Int. Conf. Commun. (ICC)*, May 2016, pp. 1–5.

[12] M. Alzenad, A. El-Keyi, F. Lagum, and H. Yanikomeroglu, "3-D Placement of an unmanned aerial vehicle base station (UAV-BS) for energy-efficient maximal coverage," *IEEE Wireless Commun. Lett.*, vol. 6, no. 4, pp. 434–437, Aug. 2017.

[13] L. Ferranti, F. Cuomo, S. Colonnese, and T. Melodia, "Drone cellular networks: Enhancing the quality of experience of video streaming applications," *Ad Hoc Netw.*, vol. 78, pp. 1–12, Sep. 2018.

[14] C. D. Franco and G. Buttazzo, "Energy-aware coverage path planning of UAVs," in *Proc. IEEE Int. Conf. Auton. Robot Syst. Competitions (ICARSC)*, Apr. 2015, pp. 111–117.

[15] A. Trotta, F. D'Andreagiovanni, M. D. Felice, E. Natalizio, and K. R. Chowdhury, "When UAVs ride a bus: Towards energy-efficient city-scale video surveillance," in *Proc. IEEE Conf. Comput. Commun.*, Apr. 2018, pp. 1043–1051.

[16] G. Piro, M. Miozzo, G. Forte, N. Baldo, L. A. Grieco, G. Boggia, and P. Dini, "HetNets powered by renewable energy sources: Sustainable next-generation cellular networks," *IEEE Internet Comput.*, vol. 17, no. 1, pp. 32–39, Jan./Feb. 2013.

[17] M. A. Marsan, G. Bucalo, A. D. Caro, M. Meo, and Y. Zhang, "Towards zero grid electricity networking: Powering BSs with renewable energy sources," in *Proc. IEEE Int. Conf. Commun. Workshops (ICC)*, Jun. 2013, pp. 596–601.

[18] D. Renga and M. Meo, "From self-sustainable green mobile networks to enhanced interaction with the smart grid," in *Proc. 30th Int. Teletraffic Congr. (ITC)*, vol. 1, Sep. 2018, pp. 129–134.

[19] Q. Wu, Y. Zeng, and R. Zhang, "Joint trajectory and communication design for multi-UAV enabled wireless networks," *IEEE Trans. Wireless Commun.*, vol. 17, no. 3, pp. 2109–2121, Mar. 2018.

[20] G. Bartoli, R. Fantacci, K. B. Letaief, D. Marabissi, N. Privitera, M. Pucci, and J. Zhang, "Beamforming for small cell deployment in LTE-advanced and beyond," *IEEE Wireless Commun.*, vol. 21, no. 2, pp. 50–56, Apr. 2014.

[21] *LTE-A Small Cells*. Accessed: Apr. 28, 2019. [Online]. Available: http://www.isticom.it/documenti/formazione/lte_a_small_cells_4apr2017.pdf

[22] *Ericsson Radio Dot: Evolution and Technical Information*. Accessed: Apr. 28, 2019. [Online]. Available: https://smallcells.3g4g.co.uk/2017/09/ericsson-radio-dot-evolution-and.html

[23] *Small Cell Network White Paper*. Accessed: Apr. 28, 2019.[Online]. Available: https://www.huawei.com/minisite/hwmbbf16/insights/small_cell_solution.pdf

[24] *Italy Wireless Spectrum usage Carriers*. Accessed: Apr. 28, 2019. [Online]. Available: https://lteitaly.it/it/spectrum.php

[25] D. Muirhead, M. A. Imran, and K. Arshad, "Insights and approaches for low-complexity 5G small-cell base-station design for indoor dense networks," *IEEE Access*, vol. 3, pp. 1562–1572, 2015.

[26] A. Arbi and T. O'Farrell, "Energy efficiency in 5G access networks: Small cell densification and high order sectorisation," in *Proc. IEEE Int. Conf. Commun. Workshop (ICCW)*, Jun. 2015, pp. 2806–2811.

[27] D. P. Bertsekas, *Network Optimization: Continuous and Discrete Models*. Belmont, MA, USA, Athena Scientific, 1998.

[28] S. Colonnese, F. Cuomo, L. Chiaraviglio, V. Salvatore, T. Melodia, and I. Rubin, "CLEVER: A cooperative and cross-layer approach to video streaming in hetnets," *IEEE Trans. Mobile Comput.*, vol. 17, no. 7, pp. 1497–1510, Jul. 2018.

[29] J. M. Seddon and S. Newman, *Basic Helicopter Aerodynamics*, vol. 40. Hoboken, NJ, USA: Wiley, 2011.

[30] *Small Cells: No Power, No Problem*. Accessed: Dec. 21, 2018. [Online]. Available: https://www.isemag.com/2017/09/small-cells-no-power-no-problem/

[31] B. Marion and M. Anderberg, "PVWATTS-an online performance calculator for grid-connected PV systems," in *Proc. Solar Conf.*, Colorado, CO, USA: Amer. Solar Energy Soc., 2000, pp. 119–124.

[32] *National Electricity Market Authority*. Accessed: Dec. 21, 2018. [Online]. Available: http://www.mercatoelettrico.org/En/Default.aspx

[33] *TorrinoMezzocammino from Drone*. Accessed: Apr. 29, 2019. [Online]. Available: https://www.youtube.com/watch?v=QDzZxkpoZik

[34] *Chula Vista Launches Drone as First Responder*. Accessed: Apr. 29, 2019. [Online]. Available: https://www.chulavistaca.gov/Home/Components/News/News/1826/8221
[35] *News Release: DHS S&T Seeks Innovators to Collaborate Smart Cities Technologies*. Accessed: Apr. 29, 2019. [Online]. Available: https://www.dhs.gov/science-and-technology/news/2018/01/04/news-release-st-seeks-innovators-collaborate-smart-cities

LUCA CHIARAVIGLIO (M'09–SM'16) received the Ph.D. degree in telecommunication and electronics engineering from the Politecnico di Torino, Italy. During the past years, he has spent research periods with Boston University, Boston, MA, USA; INRIA Sophia Antipolis, France; Auckland University of Technology, New Zealand; and ETECSA S.A., Cuba. He is currently a Tenure Track Assistant Professor with the Department of Electronic Engineering, University of Rome Tor Vergata, Italy. He has coauthored over 130 papers published in international journals, books, and conferences, and has collaborated with over 150 coauthors, which are affiliated with more than 40 national and international institutions. His current research interests include 5G networks, cloud computing, optimization applied to telecommunication networks, new architectures to reduce the digital divide in rural and low-income areas, and electromagnetic fields. He is currently the coordinator of the national project BRIGHT: Bringing 5G Connectivity in Rural and Low-Income Areas. During the last years, he has been involved in different European projects, such as the H2020 5G-EVE, H2020 Superfluidity, FP7 Trend, FP7 EcoNet, and FP7 Bone. He is a founding member of the IEEE Communications Society Technical Subcommittee on Green Communications and Computing. According to Google Scholar, his H-Index is 30. He participates in the TPC of top-leading conferences, including the IEEE INFOCOM, the IEEE GLOBECOM, the IEEE ICC, the IEEE VTC, and the IEEE GlobalSIP. He is a member of the organizing committee of several conferences, such as ECOC, LANMAN, and 5G-Italy. He is in the Editorial Board of the *IEEE Communications Magazine*, IEEE Access, and the IEEE Transactions on Green Communications and Networking. He has received the Best Paper Award in different conferences, including the IEEE VTC and ICIN. Some of his papers are listed as Best Readings on *Green Communications* by IEEE. Moreover, he has been recognized as an author in the top 1% most highly cited papers in the ICT field worldwide. His papers "Optimal Energy Savings in Cellular Access Networks" and "Reducing Power Consumption in Backbone Networks" are the most cited papers from all the IEEE ICC conferences and the IEEE ICC workshops, from 2009 to 2018 (Source: Scopus).

FABIO D'ANDREAGIOVANNI received the M.Sc. degree in industrial engineering, and the Ph.D. degree in operations research from the University of Rome Sapienza, in 2006 and 2010, respectively. He was a Research Scholar with the Department of Industrial Engineering and Operations Research, Columbia University in the City of New York, from 2008 to 2009. He has been a First Class Research Scientist with the French National Center for Scientific Research (CNRS) and at the Laboratory "Heudiasyc" of UTC-Sorbonne University, since 2016. Until 2016, he was the Head of Research Group, Department of Mathematical Optimization, Zuse Institute Berlin. He was also a Lecturer with the Department of Mathematics and Computer Science, Free University of Berlin, and with the Faculty of Engineering, Technical University of Berlin. He has worked as consultant for several major European telecommunications and electric utility companies. His research has been focused on the theory and applications of robust optimization and mixed integer programming and has received many awards for his work, such as the Accenture M.Sc. Prize 2006, the INFORMS Telecom Ph.D. Award 2010, the INFORMS Telecom Best Paper Award 2014, the RNDM Best Paper Award 2017, the EvoStar-EvoApplications Best Paper Award 2018, and the ICIN Best Paper Award 2018.

KIM-KWANG RAYMOND CHOO (SM'15) received the Ph.D. degree in information security from the Queensland University of Technology, Australia, in 2006. He currently holds the Cloud Technology Endowed Professorship with The University of Texas at San Antonio (UTSA), and has a courtesy appointment with the University of South Australia. He is also a Fellow of the Australian Computer Society. In 2016, he was named the Cybersecurity Educator of the Year - APAC (Cybersecurity Excellence Awards are produced in cooperation with the Information Security Community on LinkedIn). In 2015, he and his team won the Digital Forensics Research Challenge organized by the University of Erlangen-Nuremberg, Germany. He is a recipient of the 2018 UTSA College of Business Col. Jean Piccione and Lt. Col. Philip Piccione Endowed Research Award for Tenured Faculty, the ESORICS 2015 Best Paper Award, the 2014 Highly Commended Award by the Australia New Zealand Policing Advisory Agency, the Fulbright Scholarship, in 2009, the 2008 Australia Day Achievement Medallion, and the British Computer Society's Wilkes Award, in 2008.

FRANCESCA CUOMO received the Laurea degree *(magna cum laude)* in electrical and electronic engineering from the University of Rome Sapienza, in 1993, and the Ph.D. degree in information and communications engineering from the University of Rome Sapienza, in 1998, where she has been an Associate Professor with the University of Rome Sapienza, since 2005, and teaches courses in telecommunication networks. She has advised numerous master students in computer engineering, and has been the advisor of nine Ph.D. students in networking. Her current research interests focus on vehicular networks and sensor networks, cognitive radio networks, reconfigurable radio systems, and energy saving in the Internet and in the wireless systems. She has participated in several National and European projects on wireless network systems such as the RAMON, VICOM, INSYEME, IST WHYLESS, IST EPERSPACE, and IST CRUISE. She has authored over 120 peer-reviewed papers published in prominent international journals and conferences. She has been in the editorial board of the *Computer Networks* (Elsevier) and is currently a member of the editorial board of the *Ad-Hoc Networks* (Elsevier) and the IEEE Transactions on Mobile Computing. She has been the TPC Co-Chair of several editions of the ACM PE-WASUN Workshop, the Track-Chair of the IEEE WiMob2017 Symposium on Ubiquitous Computing, Services and Applications, and the Guest Editor of the Ad-Hoc Networks Special issue on the *Modeling and Performance Evaluation of Wireless Ad-Hoc Networks*, 2015.

STEFANIA COLONNESE was born in Rome, Italy. She received the Laurea degree from the University of Rome Sapienza, Italy, in 1993, and the Ph.D. degree from the University of Roma Tre, Italy, in 1997, both in electronic engineering. She has participated in the MPEG-4 standardization activity on automatic video segmentation. In 2001, she joined the University of Rome Sapienza as an Assistant Professor. Her current research interests include the areas of signal and image processing, multiview video communications processing, and networking.